Published in final edited form as:
Cell Metab. 2014 July 1; 20(1): 103–118. doi:10.1016/j.cmet.2014.05.005.

Adipocyte Inflammation is Essential for Healthy Adipose Tissue Expansion and Remodeling

Ingrid Wernstedt Asterholm[1,*], **Caroline Tao**[1], **Thomas S. Morley**[1], **Qiong A. Wang**[1], **Fernando Delgado-Lopez**[2], **Zhao V. Wang**[1], and **Philipp E. Scherer**[1,3]

[1]Touchstone Diabetes Center, Dept. of Internal Medicine, UTSW Medical Center, 5323 Harry Hines Blvd., Dallas, TX 75390-8549, USA

[2]Facultad de Medicina, Universidad Catolica del Maule, Avda. San Miguel 3605, Talca, Chile

[3]Cell Biology, UTSW Medical Center, 5323 Harry Hines Blvd., Dallas, TX 75390-8549, USA

Summary

Chronic inflammation constitutes an important link between obesity and its pathophysiological sequelae. In contrast to the belief that inflammatory signals exert a fundamentally negative impact on metabolism, we show that pro-inflammatory signaling in the adipocyte is in fact required for proper adipose tissue remodeling and expansion. Three mouse models with an adipose tissue-specific reduction in pro-inflammatory potential were generated that display a reduced capacity for adipogenesis *in vivo*, while the differentiation potential is unaffected *in vitro*. Upon high fat diet exposure, the expansion of visceral adipose tissue is prominently affected. This is associated with decreased intestinal barrier function, increased hepatic steatosis and metabolic dysfunction. An impaired local pro-inflammatory response in the adipocyte leads to increased ectopic lipid accumulation, glucose intolerance and systemic inflammation. Adipose tissue inflammation is therefore an adaptive response that enables safe storage of excess nutrients and contributes to a visceral depot barrier that effectively filters gut-derived endotoxin.

Correspondence to: Philipp E. Scherer, Touchstone Diabetes Center, Dept. of Internal Medicine, UTSW Medical Center, 5323 Harry Hines Blvd., Dallas, TX 75390-8549, USA, philipp.scherer@utsouthwestern.edu, Tel: 214-648-8715; Fax: 214-648-8720.
[*]current affiliation: Box 432, Inst. of Neuroscience and Physiology, Sahlgrenska Academy at the University of Gothenburg, 405 30 Gothenburg, Sweden

Supplemental Information
Supplemental information includes experimental procedures, six additional figures and three tables. They appear with this article online at *XXX*.

Author contributions
IWA designed the study, carried out the research, interpreted the results, and wrote the manuscript. CT, TSM, QAW, FDL and ZVW assisted in study design, performed research, and reviewed the manuscript. PES designed the study, analysed the data, reviewed and revised the manuscript, and is responsible for the integrity of this work. All authors approved the final version of the manuscript.

The authors declare no conflicts of interest.

Introduction

Adipose tissue expansion in response to excess caloric intake is an important systemic response to avoid the lipotoxic side effects exerted by excess lipid and fatty acid (FA) deposition in cells other than adipocytes. The basic mechanisms, leading to a gradual and "healthy" expansion of fat pads, are starting to be elucidated. Healthy expansion is associated with appropriate angiogenesis and vascular and extracellular matrix (ECM) remodeling.

Increased adiposity is more often than not associated with an increased risk for a number of chronic diseases, including diabetes, cardiovascular disease and some types of cancers (Park et al., 2011). The underlying mechanisms for the link between obesity and these diseases are not fully understood, but are likely to involve a state of chronic systemic low-grade inflammation.

The causality between local adipose tissue inflammation, systemic inflammation and metabolic dysfunction has however not been studied. Therefore, we developed three distinct, but complementary mouse models to investigate the role of adipose tissue inflammation in high fat diet (HFD)-induced metabolic disturbances. By design, two models express the anti-inflammatory factors in adipose tissue constitutively, while one model is inducible.

Analysis of these three mouse models reveals that the inability to mount an appropriate local pro-inflammatory response at the level of the adipocyte reduces adipose tissue expansion under normal physiological as well as under HFD-fed conditions. This inability to expand adipose tissue is associated with ectopic lipid deposition and a deteriorated metabolic profile. Furthermore, we demonstrate that mesenteric adipose tissue (MWAT, a visceral fat depot) plays an important role for proper intestinal barrier function. An ineffective response of MWAT to pro-inflammatory stimuli with respect to its expansion is associated with a "leaky gut", colitis and metabolic dysfunction. Thus, these mouse models demonstrate that a local inflammatory response derived from the adipocyte is an adaptive response and an important preemptive factor for ensuing obesity-associated systemic inflammation.

Results

We have recently developed a mouse model (the "adipochaser mouse") in which we can permanently activate β-galactosidase-expression in all preexisting adipocytes by a short bout of doxycycline-treatment. Removal of doxycycline enables the detection of newly differentiated adipocytes that are negative for the blue X-Gal-LacZ staining (Wang et al., 2013). Repeated local LPS injections into adipose tissue stimulate adipogenesis without affecting overall weight gain (Sadler et al., 2005). Exploiting our adipochaser mouse, we are able to confirm the findings by Sadler and colleagues. New adipocyte formation was evident in the LPS-injected inguinal WAT (IWAT) depot, but not in the control depot (Fig. 1A and data not shown). These observations suggest that the induction of acute inflammation in the context of intact adipose tissue stimulates adipogenesis *in vivo*. We therefore hypothesized that acute inflammation within adipose tissue may play an essential role for adipose tissue expansion, remodeling and overall homeostasis by stimulating ECM degradation and

angiogenesis. To study the role of inflammation in adipose tissue, we developed a mouse model expressing a dominant-negative version of the potent pro-inflammatory cytokine TNFα (dnTNF) (Steed et al., 2003) under the control of the ap2 promoter ("dnTNF tg"). This is a version of TNFα that effectively hetero-trimerizes with wildtype TNFα subunits, but the presence of a mutant subunit engages the TNF-receptors non-productively. aP2 promoter-driven constructs are predominantly transcribed in adipocytes, but expression has been reported for macrophages and other tissues, such as the heart and the brain, though at much lower levels. Our dnTNF tg mice express the transgene specifically in adipose tissue, but also to a minor extent in isolated peritoneal macrophages (Fig. S1A). The low level of dnTNF expression in macrophages does not affect the inflammatory state of thioglycollate-activated peritoneal macrophages, since a number of cytokines and M1/2 markers (e.g. TNFα, IL-1β, TGFβ, Arg1 and CD11c) remained unaltered compared to macrophages isolated from littermate controls (Fig. S1B).

As expected, unchallenged chow-fed dnTNF tg do not display significant differences with respect to genes involved in inflammation or macrophage polarization e.g. TNFα, F4/80, CD11c, NOS2, CD206 and CD301 in adipose tissue (data not shown). However, the dnTNF tg mice display a reduced NFκB activation in adipose tissue (as judged by reduced IκBα phosphorylation) in response to an intraperitoneal injection with TNFα (Fig. S1C). Furthermore, LPS induces a highly specific response on adipocytes in adipose tissue, leading to an acute increase in serum leptin levels. In the presence of dnTNF, this LPS-mediated increase in serum leptin levels is significantly blunted (Fig. 1B). This indicates that an autocrine TNFα loop is part of the LPS-mediated effects on leptin release. Even though the increase in serum SAA and α1acid-glycoprotein (Fig S1D and data not shown), the body weight recovery is slightly faster in the dnTNF tg mice (Fig. 1C). Combined, these results confirm that the dnTNF transgene is indeed functional, and that it exerts its effects primarily at the level of adipose tissue, while leaving the inflammatory response in other tissues, such as the liver, fully intact.

Reduced body weight, fat mass and glucose tolerance in HFD-fed dnTNF tg mice

In young chow-fed mice, the body weights trend to be lower in the dnTNF mice. The IWAT weight is reduced, while the gonadal WAT (GWAT) weight is similar between genotypes (Fig. 1D). This pattern changes upon HFD-feeding. The degree of HFD-induced obesity is reduced in the dnTNF mice (Fig. 1E). This is particularly apparent in GWAT, which is much more prominently affected than the IWAT depot in HFD-fed mice (Fig. 1D). In absolute terms, both GWAT and IWAT are of reduced size in HFD-fed dnTNF tg mice compared to littermates. The reduced IWAT weight is however proportional to the lower body weight in the dnTNF mice. Brown adipose tissue (BAT) and MWAT are however of similar sizes in dnTNF and littermate controls, regardless of diet (data not shown). Similar results were seen when the dnTNF transgene was bred into the genetically obese *ob/ob* background, indicating that there are leptin-independent mechanisms responsible for the reduced body and GWAT mass weight in dnTNF mice (Fig. S1E).

We went on to test whether the reduced body weight translates into the expected improvements in metabolic parameters. To our surprise, HFD-fed dnTNF tg mice are

severely glucose intolerant and have lower adiponectin levels, despite lower levels of circulating SAA compared to littermate controls (Fig. 1F-H).

These observations suggest that adipose tissue TNFα-signaling is relevant for adipose tissue remodeling and expansion. Consistent with this hypothesis, we found increased amounts of ECM deposits in IWAT of HFD-fed dnTNF mice compared to littermate controls (Fig. 1I). This result is consistent with a need for TNFα for successful ECM-remodeling in the context of wound healing (Heo et al., 2011; Saika et al., 2006). The HFD-induced adipocyte hypertrophy in IWAT is similar between genotypes (relative adipocyte sizes: 1.00 ± 0.3 and 0.94 ± 0.1 for respectively wildtype and dnTNF tg IWAT, p=0.84), despite about 60% reduced IWAT depot weight in the dnTNF tg mice (Fig 1D), suggesting that inhibition of TNFα-signaling either causes a reduced capacity for adipogenesis *in vivo*, or may simply be secondary to the increased fibrosis. Disruption of this fibrotic state, such as in the context of HFD-exposed mice lacking collagen VI (Khan et al., 2009), reduces adipocyte apoptosis. In contrast, enhanced fibrosis increases the rate of adipocyte death (Halberg et al., 2009). In line with fibrosis-induced adipocyte death, prolonged HFD-feeding (22 weeks) leads to an increased presence of crown-like structures (CLS's) in the GWAT of dnTNF tg mice. This is apparent when examining infiltrating macrophages (as judged by Mac2-staining) surrounding dead adipocytes (as judged by perilipin-negative staining) (Fig. 1J). We did however not detect a difference in adipocyte death in IWAT and no difference was observed in GWAT at earlier stages of HFD-feeding (data not shown). Thus, a reduction in adipogenesis is more likely to explain the enlarged adipocytes in IWAT and the reduced GWAT size in HFD-fed dnTNF tg mice.

Essential role for acute inflammation for adipose tissue functionality

Given the many studies showing the negative impact of TNFα on insulin sensitivity as well as on adipocyte differentiation (Engelman et al., 2000; Gustafson and Smith, 2006; Hotamisligil et al., 1993), the metabolic and adipose tissue dysfunction seen for the dnTNF tg mice is rather surprising at first sight. However, our observations do not contradict a model in which *chronic* inflammation is an important contributor towards the metabolic syndrome. Rather though, "immunologic fitness" as we have previously defined it (Asterholm et al., 2012), seems to be an important component for tissue homeostasis in general and for adipose tissue in particular. To further explore this concept of "physiological adipose tissue inflammation", we wanted to test an additional model to strengthen the general validity of our initial findings in these dnTNF tg mice. To do so, we generated a more potent adipose-specific anti-inflammatory model. This second mouse model takes advantage of RIDα/β (RID), an adenoviral protein complex that suppresses the local host immune response by potently inhibiting a number of pro-inflammatory signaling pathways (e.g. TLR4-, TNFα- and IL-1β-mediated signaling) (Lichtenstein et al., 2004). Similar to the dnTNF tg mice, we put the expression of RID under the control of the aP2 promoter (RID tg). Just as for the dnTNF tg mouse model, we detected a high transgene expression in adipocytes with low level expression also seen in macrophages, but not in other tissues (Fig. S2A). Upon isolating fresh peritoneal thioglycollate-stimulated macrophages from wildtype and RID mice, we did not detect any functional differences in isolated and cultured macrophages, suggesting that the trace levels of expression do not amount to an effective

suppression of inflammation in macrophages (Fig. S2B**)**. Consistent with a potent action within the adipocyte, the RID tg mice display a significantly blunted response to LPS in adipose tissue, associated with a reduced response to LPS-induced body weight loss as well (Fig. 2A and B). Moreover, and also similar to the dnTNF tg mice, fad pad weights of the RID tg mice are reduced. The more effective anti-inflammatory effects in the RID tg lead to a significant reduction in both IWAT and GWAT depot sizes, even in young chow-fed mice (Fig. 2C). HFD-feeding causes an even more dramatic difference with respect to the visceral GWAT and MWAT depots, while the subcutaneous IWAT depot no longer differs in size from the wildtype controls under these conditions (Fig. 2D). BAT weights are similar between genotypes, with or without HFD-challenge (data not shown). Despite the reduced overall amounts of white adipose tissue, the RID tg mice do not display altered overall body weight (Fig. S2C)**.**

Body composition, as assessed by NMR, confirmed a slightly reduced fat mass in both the dnTNF and the RID tg mice compared to wild type controls, and as little as two days of HFD-feeding enhances this difference between genotypes (Fig. S2D and E). Lean body mass was however unaltered in both mouse models (Fig. S2D and E). We also investigated whether these transgenic mice display an altered energy balance, but neither food intake nor oxygen consumption differed from their respective controls (data not shown). Thus, the reduced body weight in the dnTNF must be caused by an alteration in energy balance that is too small to be detected with available methods. In contrast, the respiratory quotient ($RQ=VO_2/VCO_2$) was significantly altered. HFD-fed dnTNF tg mice display a lower RQ in the dark phase and the RID tg mice display a lower dark phase-RQ on both chow and HFD. This reduction in RQ in both dnTNF and RID tg mice compared to their controls indicates a heavier reliance on fatty acid oxidation for their energy need (Fig. S2F and G). Typically, healthy mice burn carbohydrates during the dark phase. At this time of day, they have the highest food intake and hence the highest insulin levels. Thus, a the lower RQ during the dark phase, reflective of reduced carbohydrate use, is an indication of systemic insulin resistance and metabolic inflexibility in both transgenic strains.

The inhibition of adipogenesis (as gauged by the estimated number of adipocytes) is even more pronounced in the RID tg mice **(**Fig. 2E**)**. Chow-fed RID tg mice display 17 ± 2 % larger adipocytes in IWAT ($p<0.05$) and a trend towards larger adipocytes in GWAT (27% ± 11 larger, $p=0.14$) despite the fact that these depots are 25% (IWAT) and 30% (GWAT) smaller than in wild type controls **(**Fig. 2C**)**. The circulating SAA levels are to our surprise higher in chow-fed RID tg mice, but this difference disappears on HFD i.e. the HFD-induced increase in SAA is more pronounced in wild type mice (Fig. S2H). Similar to the dnTNF tg mice, the RID tg adipose phenotype is associated with both reduced adiponectin levels and glucose intolerance (Fig. 2F-G). In fact, RID tg mice have a substantial degree of glucose intolerance with mild hyperinsulinemia already under unchallenged, chow-fed conditions at a young age. It could very well be that the lower adiponectin levels contribute to this impaired insulin sensitivity. HFD-feeding aggravates the metabolic phenotype further, and the RID tg mice continue to display reduced glucose tolerance despite severe hyperinsulinemia relative to the wildtype controls (Fig. 2H-I). Upon closer analysis of the adipose tissue, we found elevated levels of collagen in HFD-fed RID tg IWAT.

Interestingly, in these experiments, we noticed that HFD induces a rapid and dramatic reduction of septa in IWAT. These septa are easily detectable with a Picrosirius red stain, while somewhat less apparent with Trichrome stain, and correspond to collagen streaks that compartmentalize adipose tissue "units" in young wildtype mice (Fig. 3A **and** Fig. S3A). There is no description in the literature of either the developmental origin or the relevance of these functional "mini-units" in adipose tissue. The reduction in septa can be quantified by total collagen measurements. HFD-fed wildtype, but not RID tg mice, have a reduced total amount of collagen per mg adipose tissue compared to the levels in chow-fed controls (Fig. 3B). Thus, adipose tissue fibrosis in obesity may, at least in some cases, be the consequence of reduced ECM-degradation, rather than an increase in ECM production. We should also note that total collagen content measurements of adipose tissue do not necessarily reflect states of pathological fibrosis, since healthy chow-fed mice have higher levels of collagen in IWAT than metabolically challenged obese mice. Instead, these data suggest that beyond biochemical measurements, a histological examination also has to be performed to accurately assess whether a pathological condition prevails (e.g. the collagen deposits show up as irregular streaks or in association with crown-like structures) or whether the collagen deposits are in the form of well-organized septa, as seen in the lean animals.

Reduced HFD-induced adipose tissue expansion in dnTNF and RID tg mice is associated with hepatic steatosis

These initial observations support the hypothesis that the ability to mount a pro-inflammatory response is intimately coupled to adipose tissue expansion, proper remodeling and the resolution of inflammation. We therefore wanted to determine whether the reduced storage capacity in adipose tissue leads to increased ectopic lipid deposition. Indeed, both the dnTNF and the RID tg mice display an increased degree of HFD-induced hepatic steatosis (Fig. 3C-D). Given the blunted HFD-induced weight gain in the dnTNF tg mice and the higher anti-inflammatory potency of the RID transgene, it is not surprising that the effects on the liver are more severe in the RID tg mice. In addition to the increased amounts of liver fat, RID tg mice also display a high level of hepatomegaly during HFD-fed conditions (Fig. 3D). Thus, the increased ectopic lipid deposition in dnTNF and RID tg mice can, at least in part, explain the more severe degree of HFD-induced metabolic dysfunction compared to controls in these mouse models.

Adipocyte inflammation is important for early postnatal adipogenesis

The observations so far argue that the reduced adipose tissue mass in the dnTNF and the RID tg mice is the consequence of a decreased adipogenesis rate, partially offset by a more pronounced hypertrophy of existing adipocytes. Moreover, the reduced overall fat mass cannot solely be the consequence of an altered energy balance since only the dnTNF, but not the RID transgenic mice display lower body weights; and adipose depot sizes in both the dnTNF and the RID tg mice are disproportionately reduced beyond what is expected from the body weight differentials to wildtype mice. We were therefore prompted to further explore the phenomenon of reduced adipose expansion and remodeling in these anti-inflammatory models. First, we explored whether adipogenesis is already negatively affected during postnatal development. Immediately at birth, wildtype mice rapidly expand their IWAT depots. IWAT pads grow substantially within 1-2 weeks, while the visceral

adipose depots remain almost undetectable at this young age. We measured the differences in adipose tissue size in 10-day old pups. Indeed, the RID tg pups display fewer, but larger adipocytes in developing IWAT, while body weights are unaltered compared to wildtype controls (Fig. 3E-F and data not shown). This difference is associated with a decrease in vascular density as judged by IHC stains of endomucin of IWAT (Fig. 3E-F). The dnTNF mice display a similar, albeit less dramatic, phenotype. The 10-day old dnTNF tg pups have a slightly reduced total body weight, though the IWAT weight is reduced both in relation to body weight and in absolute terms compared to littermate controls (Fig. 3G). The dnTNF adipocytes in GWAT are larger, while the adipocytes in IWAT are of similar size compared to wildtype adipocytes on postnatal day 10 (Fig. 3G). Even the dnTNF tg mice have therefore a reduced number of adipocytes, since the adipose depots are overall smaller. There is no evidence of dead adipocytes in either GWAT or IWAT in any of the genotypes (Fig S3B **for RID tg** and dnTNF tg data not shown).

A concern in this context is that both RID tg and dnTNF could lead to inhibition of adipogenesis due to cytotoxic effects or due to unspecific interference with the differentiation program. To investigate this possibility, we isolated stromal vascular cells from IWAT of wildtype, dnTNF and RID tg mice, propagated them in culture and then subjected the cells to an *in vitro* differentiation protocol and assessed the degree of differentiation by several different criteria (Fig. S3C-E). All three cell preparations differentiated to the same extent as judged by appearance of lipid droplets in bright field microscopy (Fig. S3C), Oil Red O staining (Fig. S3D) and by immunoblotting for the adipocyte marker adiponectin (Fig. S3E). Thus, the reduced adipogenic potential in the transgenic mice is truly a function of the reduced ability of these cells to respond to external pro-inflammatory stimuli in the context of an intact adipose tissue depot, rather than a cell-autonomous differentiation defect due to transgene expression.

The first few postnatal days are associated with an increased exposure to many new antigens due to microbial colonization of the gut, concomitant with a sudden intake of large quantities of milk. A large intake of lipids has been shown to acutely cause inflammatory responses in various tissues, including adipose tissue (Asterholm et al., 2012; Magne et al., 2010). We hypothesize that the likely increase in the systemic levels of bacterial toxins further elevates the lipid-induced pro-inflammatory response, and facilitates angiogenesis that in turn is permissive for adipogenesis (Fig. S4A). Hence, we suggest that gut bacteria play a major role in proper storage of excess nutrients during this early postnatal stage. To test this hypothesis, we exposed wildtype and RID transgenic mice for five weeks prior to mating to a chow diet supplemented with antibiotics that effectively deplete the commensal microflora (Rakoff-Nahoum et al., 2004). The antibiotics were removed from the food between E0-16 and re-introduced again at day E17 to avoid potentially harmful effects of these drugs on fetal development. There was no effect on the offspring's body weight, neither by antibiotics nor by genotype, and all pups survived and appeared healthy regardless of treatment group. We found that antibiotic-treated wildtype offspring display reduced amounts of adipose tissue at 10 days of age compared to the untreated control mice. The RID tg pups display a reduced amount of adipose tissue relative to wildtype mice, regardless of whether they were on antibiotics or not (Fig. 4A). Thus, the presence or

absence of bacterially-derived toxins in the RID tg pups has no effect on adipose tissue growth, supporting the notion that a local inflammatory response is an important component of normal adipose tissue expansion. Furthermore, the male breeders used in this study were sacrificed after five weeks of treatment and their MWAT was collected for histological analysis. We found that antibiotic-treated wildtype mice have a reduced capillary density in their MWAT compared to controls (Fig. 4B). This observation provides additional support for the idea that bacterially-induced inflammation leads to increased angiogenesis, at least locally in MWAT (Fig. S4B). RID tg mice had a reduced capillary density, even in the absence of antibiotic treatment (Fig. 4B). Furthermore, the average MWAT adipocyte size is 20 ± 5% ($p<0.05$) larger while the MWAT depot weight is 73 ± 7% reduced, indicating a dramatic reduction in the number of MWAT adipocytes in RID tg mice compared to wild type controls. Antibiotic treatment did not have an impact on adipocyte size, but tended to reduce the capillary density even further in the RID tg MWAT, suggesting that additional cells beyond adipocytes play a role in the response to microbial toxins in adult MWAT (Fig. 4B).

Reduced adipogenesis and HFD-induced glucose intolerance in an inducible adipocyte-specific anti-inflammatory model

Since the effects seen adipose tissue expansion and metabolic health were quite striking in the RID tg and dnTNF mice, we wanted to test whether we can see a similar phenomenon in an adipocyte-specific inducible model. To that end, we generated a mouse that expresses a mutated human IκBα(S32G-S36A) version under the control of a tet-responsive element (TRE-IκB tg). IκBα(S32G-S36A) is an effective inhibitor of the NFκB pathway. This TRE-IκB tg model was crosses with transgenic mice expressing the “tet-on” transcription factor rtTA under the control of the highly adipocyte-specific adiponectin promoter (Ad-rtTA tg) (Wang et al., 2010). Upon exposing Ad-rtTA-TRE-IκB tg mice to doxycycline, κBIα(S32G-S36A) mRNA gets selectively induced in adipocytes, whereas no expression is observed in other tissues, such as the liver (Fig. S4C**).** When we analyzed the impact of the expression of this anti-inflammatory protein during late gestation and the first 10 days of the postnatal period by exposing both wildtype and transgenic dams to doxycycline, the pups expressing IκBα(S32G-S36A) displayed a reduced IWAT weight while no effect on body weight was observed (Fig. 4C). The adipocyte sizes were however similar between genotypes (data not shown), arguing for lower total number of inguinal adipocytes in 10 day-old Ad-rtTA-TRE-IκB tg pups. Similar to the other models, there was no evidence of any dead adipocytes, as judged by perilipin stain (data not shown).

We investigated the metabolic phenotype of Ad-rtTA-TRE-IκB tg mice. We found no difference between genotypes in either body weight or glucose tolerance on doxycycline-supplemented chow (data not shown). Challenging the mice with HFD for 8 weeks revealed however a significant difference between genotypes. Ad-rtTA-TRE-IκB tg mice were more glucose intolerant than littermate controls, despite comparable body weights (Fig. 4D). Similar to the dnTNF and the RID tg mice, the GWAT weight was reduced while the liver weights were increased in the HFD-fed Ad-rtTA-TRE-IκB mice (Fig. 4E). In contrast, there was no difference in IWAT, MWAT and BAT weights (Fig. 4E and data not shown). To assess whether the Ad-rtTA-TRE-IκB mice are more susceptible to develop HFD-induced

hepatic steatosis, livers were harvested from a second cohort of mice after 1, 6 and 10 weeks on doxycycline-supplemented HFD. We found a strong trend towards increased HFD-induced hepatic steatosis in relation to body weight (Fig. S4D). These findings confirm, in a third independent system, that the inability to mount a pro-inflammatory response in adipose tissue impairs adipose tissue expansion associated with metabolic dysfunction.

Impaired β_3-Adrenergic Receptor (AR) agonist-induced adipose tissue remodeling in RID tg mice

The adipose tissue response to chronic β_3-AR agonist involves a transient acute bout of inflammation and, over time, triggers "browning" of the IWAT as defined by an increased number of multilocular cells expressing uncoupling protein (UCP)-1 (Granneman et al., 2005; Mottillo et al., 2010). There is also evidence for increased adipogenesis in GWAT in response to chronic β_3AR-agonist treatment (Lee et al., 2012; Wang et al., 2013). We aimed to investigate whether adipose tissue "beiging" depends on a pro-inflammatory response. We examined one of our models, the RID tg mice and exposed them and their wildtype controls to daily β_3AR-agonist and bromodeoxyuridine (BrdU) injections for 10 days. Rather dramatic differences were apparent with respect to the response to this chronic β_3AR-agonist treatment. Wildtype adipose tissues displayed a much "browner" color than the RID tg adipose tissue (Fig. 5A), and IWAT contained a large number of multilocular adipocytes, while RID IWAT only displays a modest response in this respect (Fig. 5B). In line with these observations, the resulting UCP-1 mRNA levels are also reduced in both IWAT and GWAT the RID tg mice (Fig. S5A). Furthermore, very few BrdU-positive adipocytes were found in GWAT after chronic β_3AR-agonist in RID tg mice, while several positive cells are found in the wildtype GWAT (Fig. 5C). We measured β_3-AR mRNA expression as well as the acute lipolytic response to β_3AR-agonist treatment and found no difference in β_3-AR expression (Fig. S5A**)**. The β_3AR-agonist-induced serum FFA increase is just marginally affected in the RID mice (Fig. S5B**)**. This eliminates receptor abundance and activity as a trivial explanation for these findings. Along the same rationale, receptor abundance and signaling are therefore unlikely to explain the differences in β_3-AR agonist-induced "beiging" between genotypes. We have previously reported that inducible adipocyte-specific expression of VEGF-A leads to a "browning" of adipose tissue, similar to the effects reported for chronic β_3-AR agonist treatment (Sun et al., 2012). Therefore, we speculated that the lack of β_3-AR agonist induced-"beiging" in the RID tg mice may relate to a reduced ability to induce pro-angiogenic mediators. Indeed, upon examining the gene expression response in IWAT within 3 hours of a single dose of β_3-AR agonist, we find a blunted induction of several pro-inflammatory cytokines in the RID tg mice (Fig. 5D). Furthermore, the mRNA expression levels of classical pro-angiogenic mediators, such as VEGF-A, angiopoetin-1 and -2 (Angpt1 and Angpt2) are also reduced in the β_3-AR agonist treated RID tg mice (Fig. 5D). Notably, we did not detect an acute β_3-AR agonist-mediated *induction* of these pro-angiogenic mediators in the wildtype mice. Rather, the difference between genotypes relates mainly to a *down-regulation* of these particular genes in response to β_3-AR agonist in the RID tg mice. Thus, in the context of acute β_3-AR agonist stimulation, it seems that a potent inflammatory response is necessary to maintain the expression of VEGF-A, Angpt1 and Angpt2 in IWAT. A comparable gene expression

pattern was also seen in GWAT, albeit the individual variation is larger than in IWAT (Fig. S5C).

The reduced MWAT expansion in the RID tg mice is associated with a "leaky gut"

The RID tg mice have a more severe metabolic phenotype than the dnTNF tg and the Ad-rtTA-TRE-IκB tg mice. It caught our attention that the dnTNF tg and the Ad-rtTA-TRE-IκB tg mice display a normal HFD-induced MWAT expansion and mesenteric adipocyte size (data not shown). In contrast, MWAT expansion is dramatically reduced in the RID tg mice (Fig. 2D). This indicates that inhibition of inflammatory signaling in our mouse models is compensated for by an increase in other inflammatory signaling pathways in the mesenteric area. These compensatory mechanisms are however not present or effective in GWAT or IWAT. Moreover, the glucose intolerance seen in young unchallenged RID tg mice cannot be explained by hepatic steatosis, since comparably low levels of hepatic lipids are seen between chow-fed wildtype and RID tg mice, at least while the body weights are <30 grams (Fig. 6A). We noted, however, that SAA-levels are increased and both the liver size as well as the average size of the individual hepatocytes, are enlarged in the chow-fed RID tg mice, even in the absence of steatosis (Fig. S2H and Fig. 6B-C). Furthermore, the spleens of the RID tg mice are also enlarged (Fig. 6D). Taken together, these observations argue for a state of elevated hepatic stress and increased systemic immune activation in the RID tg mice. A likely explanation for these phenomena is an increased exposure to bacterial toxins that are leaking out from the gut. In line with this hypothesis, we found elevated levels of anti-LPS IgGs and increased intestinal permeability as judged by the circulating levels of FITC-dextran after an oral load in young RID tg mice (6-8 week old with a body weight of ≤ 20g) on a chow diet (Fig. 6E-F). Treatment with 2% dextran sulfate sodium (DSS) through drinking water, which damages the colonic epithelium, increases permeability and causes colitis, leads to a further elevation of anti-LPS IgGs levels and serves as a positive control for the plasma anti-LPS IgG assay (Fig. 6E). The colons of the DSS-treated RID tg mice display increased pathological changes, such as an increased degree of colon hyperplasia, more severe crypt disruption and leukocyte infiltration and further increased spleen size compare to the DSS-treated wildtype mice (Fig. 6G-H). Furthermore, the DSS-treated RID tg mice have increased expression of CD14, TLR4, TNFα, MCP-1, MIP-1α, F4/80 and MPO mRNA in colon, which supports the histological findings and indicates that there is a higher degree of inflammation, with enhanced recruitment/infiltration of macrophages and neutrophils, compared to the DSS-treated wildtype mice (Fig. 7A). It should also be noted that even the non-DSS treated RID tg mice display mild colon hyperplasia and elevated colon expression of CD14 and SAA3 mRNA (Fig. 6G and 7A).

Despite the lack of an effect on body weight, DSS-treatment does however impair glucose tolerance in regular wild type mice (Fig. S6A). This suggests that impaired intestinal barrier function alone (even in the absence of HFD) can have a negative impact on systemic metabolic regulation. This also suggests that at least some of the RID tg phenotype may be improved if exposure to bacterial toxins is limited. We put this hypothesis to the test and found that indeed, a 5-week antibiotics treatment normalizes spleen size and insulin levels in the transgenic mice (Fig. 7B-C). To a large extent, the expression of the liver acute phase reactants SAA-1 and -2 is also lowered to levels seen in the untreated wildtype mice (Fig.

7D). These data suggest that RID tg mice suffer from impaired intestinal barrier function, leading to “leaky gut” and colitis. This also provides an explanation for their hepatomegaly, spleen enlargement and glucose intolerance, even in the absence of an exogenous inflammatory challenge.

In contrast to the RID tg mice, the dnTNF tg and the Ad-rtTA-TRE-IκB tg mice with their associated normal MWAT expansion, do not display hepatomegaly, enlarged spleen or colon hyperplasia (data not shown). This leads us to conclude that MWAT inflammation and its subsequent expansion is an adaptive response that plays a significant role in sustaining proper intestinal barrier function and healthy symbiosis between the commensal microflora and the host.

The intestinal barrier is however not only preventing bacterial toxins from leaking out, but it also contributes to a healthy symbiosis with colonizing bacteria. An impaired intestinal barrier and/or chronic inflammation may lead to unfavorable shifts in microbial composition. This is based on the observation that gut flora can be transferred from mouse to mouse and affect the pathogenesis of obesity and hepatic steatosis (Garrett et al., 2010; Henao-Mejia et al., 2012). As expected, we found a difference in bacterial composition as judged by qPCR analysis of 8 different bacterial strains of DNA isolated from cecal content from wildtype and RID tg mice housed in different cages. Cecal levels of *Lactobacillus murinus, Mucispirillum Schaedleri* and *Eubacterium Plexicaudatum* were increased and there was a trend for reduced levels of *Firmicutes sp.*. In contrast, the levels of *Lactobacillus sp.*, *Clostridium sp. and B. Distasonis-Porphyromonas* were similar between RID tg and wild type mice (Fig. S6B). Differences in bacterial composition are not necessarily a reflection of a direct negative effect of the RID tg transgene on intestinal barrier function, but can also be secondary to metabolic disturbances and also differ between litters and cages. Importantly, the metabolic dysfunction in RID tg is apparent regardless of whether the mice under comparison are littermates or not. Furthermore, there is no difference in neither HFD-induced body weight gain, glucose tolerance, insulin levels nor hepatic steatosis in wildtype mice co-housed with either unrelated wildtype mice or with RID tg (data not shown). Thus, the potential negative effect of an altered bacterial composition in the RID tg mice is not potent enough to have an impact on metabolic health in the context of a normal immune defense in wildtype mice. We can also conclude that the wildtype gut flora does not offer a significant protective effect on the metabolic phenotype in the RID tg mice.

Discussion

The data presented here argues that a reduced ability to sense and respond to pro-inflammatory stimuli at the level of the adipocyte decreases the capacity for healthy adipose tissue expansion and remodeling. This inability results in increased HFD-induced hepatic steatosis and metabolic dysfunction. Interestingly, while the ability to sense pro-inflammatory cues that trigger expansion is of importance for all fat pads, a deficiency in this regard has particularly profound consequences for the functionality of the MWAT in the visceral depot. We observe that the lack of MWAT expansion is associated with increased

intestinal permeability and colitis, resulting in chronic systemic inflammation and metabolic dysfunction, even in the absence of HFD.

The underlying mechanism for inflammation-induced adipose tissue expansion

Adipose tissue expands either through hypertrophy of existing adipocytes or adipogenesis, i.e. differentiation of new adipocytes from adipogenic precursor cells. All models studied here establish a reduced number of adipocytes in most depots examined. Chronic HFD-feeding leads to a more pronounced GWAT depot weight difference, while the IWAT depot weight differences between tg and wildtype mice are reduced. Nevertheless, both GWAT and IWAT depots are at all times populated by fewer adipocytes in the transgenic mice than in the wildtype mice, reflecting a reduced rate of adipogenesis. Thus, the ability to mount an acute inflammatory response is playing a more important role in facilitating adipogenesis than in adipocyte hypertrophy.

The concept of inflammation-driven adipogenesis may seem contradictory at first, since pro-inflammatory cytokines, such as TNFα, are lipolytic and block adipocyte differentiation *in vitro* (Gustafson and Smith, 2006). The situation *in vitro* is however substantially different from the situation *in vivo*, since there is neither a need for angiogenesis nor ECM remodeling under *in vitro* conditions. In fact, several older studies support a role of local inflammation in increased adipogenesis. For instance, Sadler and colleagues show that low-dose LPS leads to adipocyte hyperplasia at the site of administration (Sadler et al., 2005), and there is a selective increase in the amount of MWAT in Crohn's disease as well as in experimentally-induced colitis (Gambero et al., 2007; Sheehan et al., 1992). Moreover, a very recent study on proliferation and differentiation of PDGFRα$^+$ adipocyte progenitors *in vivo* demonstrates that different adipogenic conditions are associated with an up-regulation of different sets of inflammatory and macrophage-associated genes in white adipose tissue (Lee et al., 2013).

It is likely that several distinct mechanisms contribute towards the inflammation-driven adipogenic response, with several interconnected processes triggering adipose tissue growth. Here, we found that HFD feeding acutely (within days) leads to a reduction of the total levels of collagen in IWAT in wildtype mice, but not to the same extent in the dnTNF and the RID tg mice. Thus, healthy adipose tissue expansion is associated with a net loss of adipose tissue collagen while dysfunctional adipose tissue in more advanced obesity display an increased number of ECM deposits, along with chronic inflammation and hypoxia. The inability to effectively degrade ECM limits the capacity for healthy adipose tissue expansion. RID tg adipose tissue also has a reduced capillary density. In line with this finding, the capillary density of wildtype MWAT gets reduced by ablation of gut microbiota. These data demonstrate that pro-inflammatory responses in adipose tissue are essential for both proper ECM-remodeling and angiogenesis, two processes known to facilitate adipogenesis *in vivo* and therefore are likely mediators of the inflammation-induced adipose tissue expansion phenomenon (Cao, 2007; Cristancho and Lazar, 2011).

Chronic systemic inflammation interferes with optimal metabolic fitness. However, in light of our findings in three independent adipocyte anti-inflammatory models (summarized in Table S1**)**, the view of adipose inflammation as a driving force for systemic inflammation

and metabolic dysfunction is an oversimplification. Rather, we postulate that a potent acute inflammatory response is essential for adipose tissue protection, remodeling, and expansion (Fig. 7E). This facilitates the return to a healthy equilibrium with metabolic homeostasis that subsequently allows the inflammation to reach resolution as opposed to becoming chronic.

Experimental Procedures

Animals

Adipochaser mice were described in (Wang et al., 2013). aP2-dnTNF, aP2-RID and TRE-IκBα(S32G-S36A) transgenic mice were used in a pure C57B6/J (dnTNF and TRE-IκB) or on a FVB background (RID). Mice were maintained on a 12 hour dark/light cycle and housed in groups of 4-5 with unlimited access to water, chow (No. 5058, Lab-Diet) or high fat diet (HFD) (No. D12492, Research Diets Inc as indicated for the individual experiments. In all experiments, littermate controls were used unless specifically stated otherwise. The Institutional Animal Care and Use Committee of the University of Texas Southwestern Medical Center, Dallas, has approved all animal experiments.

LPS-induced adipogenesis

Adipochaser mice were fed doxycycline-supplemented chow (600mg/kg) for one week and were thereafter switched to regular chow three days prior the experiment. The right inguinal adipose tissue (IWAT) depot of adipochaser mice were injected twice a week for two weeks with 20μg lipopolysaccharide (LPS, Sigma, USA) in 50μL PBS, while the left IWAT depot remained untreated. Five weeks later, tissues were harvested for X-Gal-LacZ staining (performed as previously described (Wang et al., 2013)).

LPS and TNFα response *in vivo*

The mice received one intraperitoneal injection with 0.3 mg/kg LPS in PBS or 0.5 μg/mouse TNFα (recombinant mouse TNFα, Biolegend, USA) in PBS supplemented with 1% BSA. Blood was collected from the tail at indicated time points.

Oral glucose tolerance test

The mice were fasted for 3 hours during the light phase and blood samples were drawn from the tail vein before and 15, 30, 60 and 120 minutes after an intragastric load with 2.5 g/kg glucose in PBS.

Adipose tissue collagen levels measurements

Pieces of inguinal adipose tissue (~50mg) were snap-frozen in N_2 (l) until analysis. The total collagen content was measured, using a commercial kit (QuickZyme Biosciences, Netherlands).

Hepatic Steatosis measurements

Quantification of hepatic steatosis was performed by computerized tomography (CT) or standard biochemical tissue triglyceride analysis. The CT analysis was performed as previously described (Asterholm and Scherer, 2010). In brief, mice were anesthetized with

Isoflurane and a CT-scan was performed at a resolution of 93 μm using the short scan mode (180°) on an eXplore Lo cus *in vivo* MicroCT Scanner from GE Healthcare. Liver lipid content was estimated by obtaining the average CT-value in multiple regions well within the liver, as validated in (Asterholm and Scherer, 2010).

Intestinal permeability assay *in vivo*

The mice were fasted for 5h; thereafter they were given an oral load with 0.6mg/g FITC-labeled dextran (average mole weight 4000, Sigma, USA). Blood samples were collected at indicated time points and the serum was diluted 2 times in PBS and loaded together with known standards diluted in 50/50 PBS/control serum on a 96-well plate and analyzed ($485nm_{ex}$, $535nm_{em}$) on a POLARstar Optima Analyzer.

Statistical Analysis

Data are in generally expressed as mean +/− standard error of the mean (SEM). The Student's t-test and 1 or 2-way ANOVA (repeated measurement) were used for comparisons between groups, log-transformation was performed as necessary to obtain normal distribution. SPSS software (version 21) was used for these statistical calculations and a p-value <0.05 was considered as significant and is indicated by a single asterisk; double asterisk: $p<0.01$; triple asterisk: $p<0.001$.

Supplementary Material

Refer to Web version on PubMed Central for supplementary material.

Acknowledgments

We would like to thank Dr. David E. Szymkowski from Xencor Inc. for providing the cDNA constructs encoding dnTNFα and for his guidance on the experimental design. We thank Dr. Bob Hammer and the Transgenic Core Facility at UTSW for the generation of the transgenic lines, Dr. Lora Hooper for advice on the antibiotics experiments, John Shelton and the Histology Core for assistance with histology and the UTSW Metabolic Core Unit for help in phenotyping. Supported by the National Institutes of Health (grants R01-DK55758, R01-DK099110 and P01DK088761-01 to PES). IWA is supported by the Throne-Holst Foundation, the Swedish Research Council (2006-3931 and 2012-1601), VINNOVA (2011-01336) and NovoNordisk Excellence Project Award. ZVW is supported by a postdoctoral fellowship from the American Heart Association (10POST4320009), QAW is supported by a postdoctoral fellowship from the American Diabetes Association (7-11-MN-47) and TSM is supported by NIH Training Grant T32-GM083831.

References

Asterholm IW, McDonald J, Blanchard PG, Sinha M, Xiao Q, Mistry J, Rutkowski JM, Deshaies Y, Brekken RA, Scherer PE. Lack of "immunological fitness" during fasting in metabolically challenged animals. J Lipid Res. 2012; 53:1254–1267. [PubMed: 22504909]

Asterholm IW, Scherer PE. Enhanced metabolic flexibility associated with elevated adiponectin levels. The American journal of pathology. 2010; 176:1364–1376. [PubMed: 20093494]

Cao Y. Angiogenesis modulates adipogenesis and obesity. The Journal of clinical investigation. 2007; 117:2362–2368. [PubMed: 17786229]

Cristancho AG, Lazar MA. Forming functional fat: a growing understanding of adipocyte differentiation. Nature reviews. Molecular cell biology. 2011; 12:722–734. [PubMed: 21952300]

Engelman JA, Berg AH, Lewis RY, Lisanti MP, Scherer PE. Tumor necrosis factor alpha-mediated insulin resistance, but not dedifferentiation, is abrogated by MEK1/2 inhibitors in 3T3-L1 adipocytes. Mol Endocrinol. 2000; 14:1557–1569. [PubMed: 11043572]

Gambero A, Marostica M, Abdalla Saad MJ, Pedrazzoli J Jr. Mesenteric adipose tissue alterations resulting from experimental reactivated colitis. Inflammatory bowel diseases. 2007; 13:1357–1364. [PubMed: 17604368]

Garrett WS, Gordon JI, Glimcher LH. Homeostasis and inflammation in the intestine. Cell. 2010; 140:859–870. [PubMed: 20303876]

Granneman JG, Li P, Zhu Z, Lu Y. Metabolic and cellular plasticity in white adipose tissue I: effects of beta3-adrenergic receptor activation. American journal of physiology. Endocrinology and metabolism. 2005; 289:E608–616. [PubMed: 15941787]

Gustafson B, Smith U. Cytokines promote Wnt signaling and inflammation and impair the normal differentiation and lipid accumulation in 3T3-L1 preadipocytes. The Journal of biological chemistry. 2006; 281:9507–9516. [PubMed: 16464856]

Halberg N, Khan T, Trujillo ME, Wernstedt-Asterholm I, Attie AD, Sherwani S, Wang ZV, Landskroner-Eiger S, Dineen S, Magalang UJ, et al. Hypoxia-inducible factor 1alpha induces fibrosis and insulin resistance in white adipose tissue. Mol Cell Biol. 2009; 29:4467–4483. [PubMed: 19546236]

Henao-Mejia J, Elinav E, Jin C, Hao L, Mehal WZ, Strowig T, Thaiss CA, Kau AL, Eisenbarth SC, Jurczak MJ, et al. Inflammasome-mediated dysbiosis regulates progression of NAFLD and obesity. Nature. 2012; 482:179–185. [PubMed: 22297845]

Heo SC, Jeon ES, Lee IH, Kim HS, Kim MB, Kim JH. Tumor necrosis factor-alpha-activated human adipose tissue-derived mesenchymal stem cells accelerate cutaneous wound healing through paracrine mechanisms. The Journal of investigative dermatology. 2011; 131:1559–1567. [PubMed: 21451545]

Hotamisligil GS, Shargill NS, Spiegelman BM. Adipose expression of tumor necrosis factor-alpha: direct role in obesity-linked insulin resistance. Science. 1993; 259:87–91. [PubMed: 7678183]

Khan T, Muise ES, Iyengar P, Wang ZV, Chandalia M, Abate N, Zhang BB, Bonaldo P, Chua S, Scherer PE. Metabolic dysregulation and adipose tissue fibrosis: role of collagen VI. Molecular and cellular biology. 2009; 29:1575–1591. [PubMed: 19114551]

Lee YH, Petkova AP, Granneman JG. Identification of an adipogenic niche for adipose tissue remodeling and restoration. Cell metabolism. 2013; 18:355–367. [PubMed: 24011071]

Lee YH, Petkova AP, Mottillo EP, Granneman JG. In vivo identification of bipotential adipocyte progenitors recruited by beta3-adrenoceptor activation and high-fat feeding. Cell metabolism. 2012; 15:480–491. [PubMed: 22482730]

Lichtenstein DL, Toth K, Doronin K, Tollefson AE, Wold WS. Functions and mechanisms of action of the adenovirus E3 proteins. International reviews of immunology. 2004; 23:75–111. [PubMed: 14690856]

Magne J, Mariotti F, Fischer R, Mathe V, Tome D, Huneau JF. Early postprandial low-grade inflammation after high-fat meal in healthy rats: possible involvement of visceral adipose tissue. The Journal of nutritional biochemistry. 2010; 21:550–555. [PubMed: 19361974]

Mottillo EP, Shen XJ, Granneman JG. beta3-adrenergic receptor induction of adipocyte inflammation requires lipolytic activation of stress kinases p38 and JNK. Biochimica et biophysica acta. 2010; 1801:1048–1055. [PubMed: 20435159]

Park J, Euhus DM, Scherer PE. Paracrine and endocrine effects of adipose tissue on cancer development and progression. Endocrine reviews. 2011; 32:550–570. [PubMed: 21642230]

Rakoff-Nahoum S, Paglino J, Eslami-Varzaneh F, Edberg S, Medzhitov R. Recognition of commensal microflora by toll-like receptors is required for intestinal homeostasis. Cell. 2004; 118:229–241. [PubMed: 15260992]

Sadler D, Mattacks CA, Pond CM. Changes in adipocytes and dendritic cells in lymph node containing adipose depots during and after many weeks of mild inflammation. Journal of anatomy. 2005; 207:769–781. [PubMed: 16367804]

Saika S, Ikeda K, Yamanaka O, Flanders KC, Okada Y, Miyamoto T, Kitano A, Ooshima A, Nakajima Y, Ohnishi Y, et al. Loss of tumor necrosis factor alpha potentiates transforming growth factor beta-mediated pathogenic tissue response during wound healing. The American journal of pathology. 2006; 168:1848–1860. [PubMed: 16723700]

Sheehan AL, Warren BF, Gear MW, Shepherd NA. Fat-wrapping in Crohn's disease: pathological basis and relevance to surgical practice. The British journal of surgery. 1992; 79:955–958. [PubMed: 1422768]

Steed PM, Tansey MG, Zalevsky J, Zhukovsky EA, Desjarlais JR, Szymkowski DE, Abbott C, Carmichael D, Chan C, Cherry L, et al. Inactivation of TNF signaling by rationally designed dominant-negative TNF variants. Science. 2003; 301:1895–1898. [PubMed: 14512626]

Sun K, Wernstedt Asterholm I, Kusminski CM, Bueno AC, Wang ZV, Pollard JW, Brekken RA, Scherer PE. Dichotomous effects of VEGF-A on adipose tissue dysfunction. Proc Natl Acad Sci U S A. 2012; 109:5874–5879. [PubMed: 22451920]

Wang QA, Tao C, Gupta RK, Scherer PE. Tracking adipogenesis during white adipose tissue development, expansion and regeneration. Nature medicine. 2013

Wang ZV, Deng Y, Wang QA, Sun K, Scherer PE. Identification and characterization of a promoter cassette conferring adipocyte-specific gene expression. Endocrinology. 2010; 151:2933–2939. [PubMed: 20363877]

Highlights

- Adipocyte inflammation facilitates adipose tissue expansion and remodeling
- Suppressed adipocyte inflammation leads to adipose tissue dysfunction
- Suppressed adipocyte inflammation leads to systemic metabolic disturbances
- Mesenteric adipose tissue is important for proper intestinal barrier function

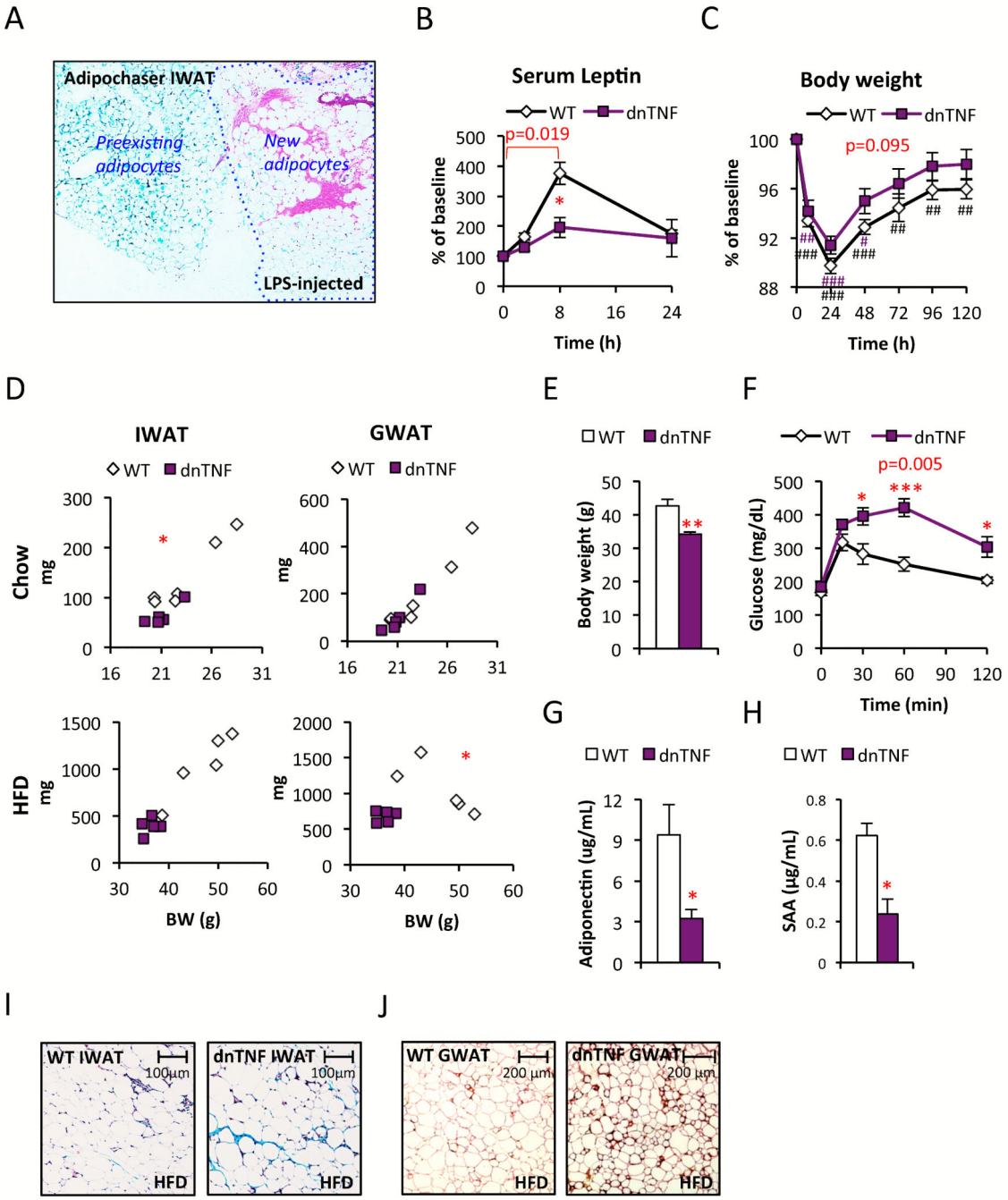

Figure 1. Reduced fat mass and glucose tolerance in dnTNF tg mice

(A) X-Gal-LacZ stained LPS-injected Adipochaser IWAT (blue=preexisting adipocytes, white=new adipocytes) (B-C) Leptin and body weight change after i.p. injection with 0.3 mg/kg LPS in dnTNF tg and wildtype female mice. (D) IWAT and GWAT weight in relation to body weight in chow (top) and HFD-fed (bottom) male dnTNF tg and wildtype controls. (E-H) Body weight, glucose tolerance test, serum adiponectin and SAA-levels in male dnTNF tg and littermate controls after 11 weeks HFD-feeding. (I) Representative Trichrome stain of IWAT in male dnTNF tg and littermate controls after 11 weeks HFD-

feeding. (J) Representative perilipin (red) and mac2 (brown) immunostain in GWAT after 22 weeks HFD-feeding in male dnTNF tg and littermate control. Error bars represent SEM, a p-value <0.05 according to student t-test was considered as significant and is indicated by */#; **/##: p<0.01; ***/###: p<0.001 (* = Difference in between genotype, # = Difference from initial weight). P-values in red indicate difference between groups during the indicated time course according to repeated measurement ANOVA.

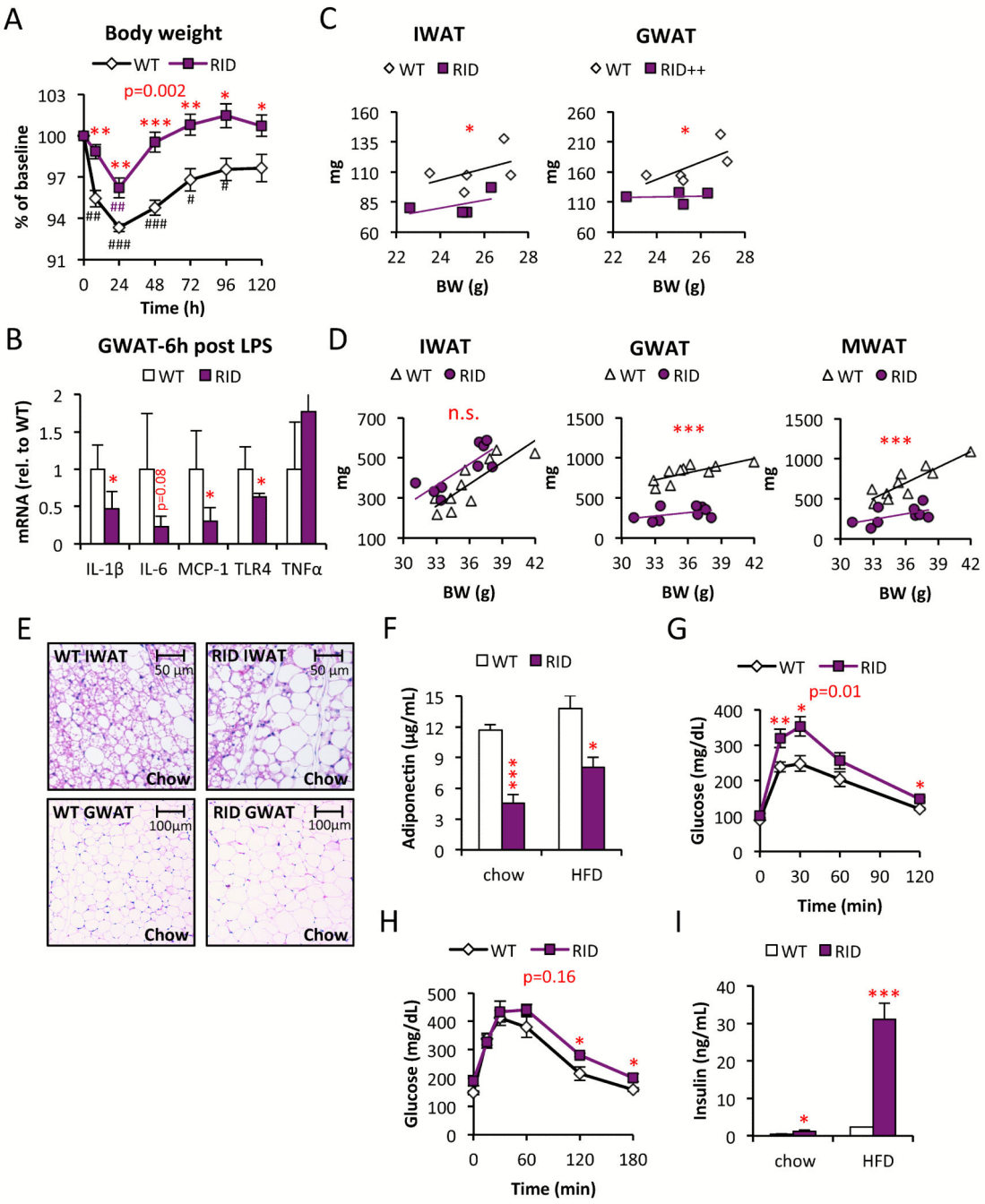

Figure 2. Reduced fat mass and reduced glucose tolerance in RID tg mice

(A) LPS (0.3 mg/kg)-induced body weight change in male RID tg and wildtype controls. (B) Gene expression in GWAT harvested from male RID tg and wildtype controls 6h after LPS injection. (C) IWAT and GWAT in relation to body weight in chow-fed male RID tg and wildtype mice. (D) IWAT, GWAT and MWAT in relation to body weight in 15 week HFD-fed male RID tg and wildtype mice. (E) Representative H&E stain of IWAT and GWAT in male RID tg and wildtype mice on chow (F) Adiponectin levels in male RID tg and wildtype mice on chow and after 12 weeks HFD. Glucose tolerance in (G) chow-fed and (H) 12-week

HFD-fed male RID tg and wildtype mice. (I) Serum-insulin levels in 3 h fasted male RID tg and wildtype mice. 1-way ANOVA analysis shows that both diet ($F=8.1$, $p=0.013$) and genotype ($F=12.3$, $p=0.004$) contribute significantly to collagen levels. Error bars represent SEM, a p-value <0.05 according to student t-test was considered as significant and is indicated by */#; **/##: $p<0.01$; ***/###: $p<0.001$ (* = Difference in between genotype, # = Difference from initial weight). P-values in red indicate difference between groups during time courses according to repeated measurement ANOVA.

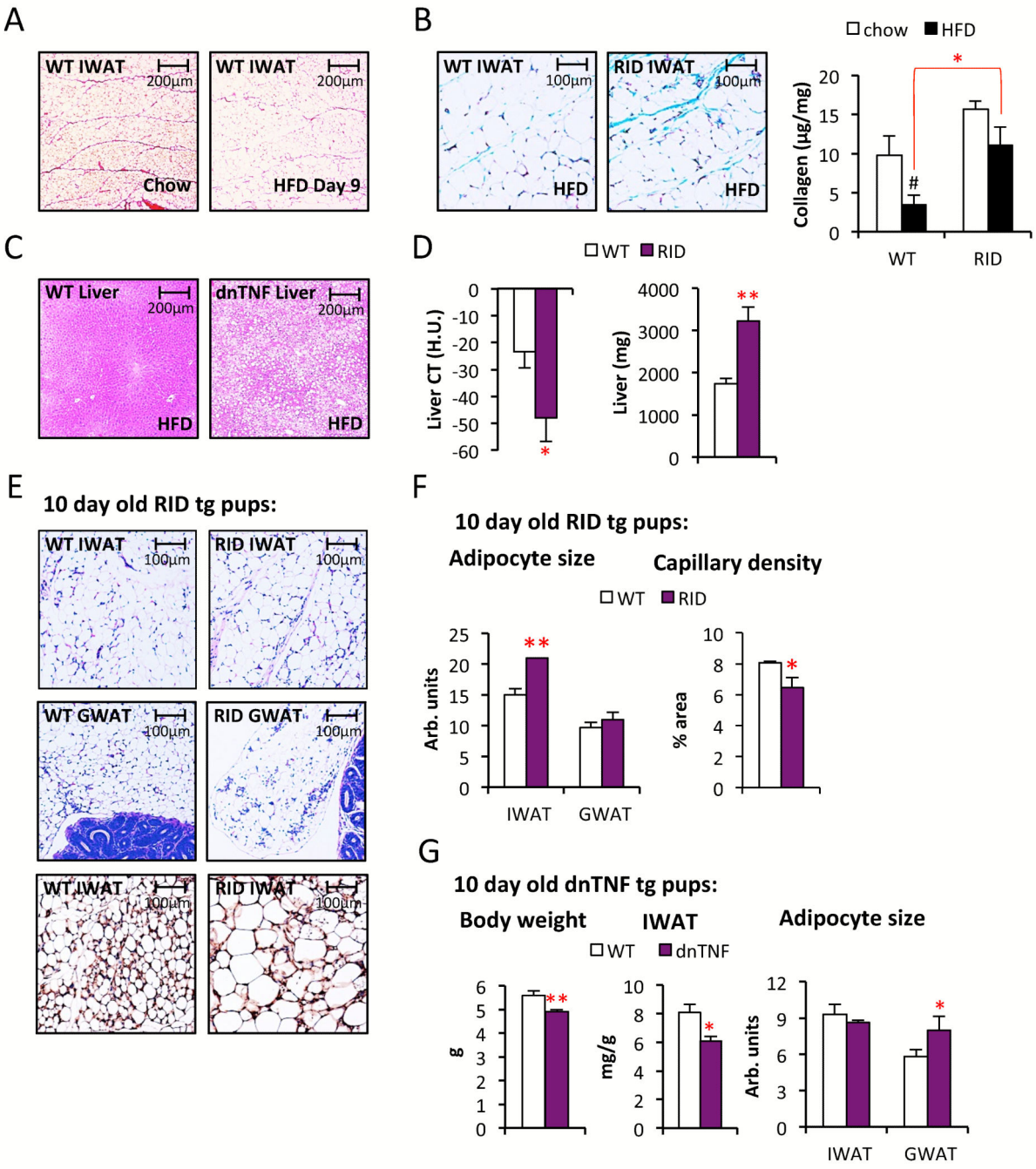

Figure 3. Increased HFD-induced steatosis and delayed adipose tissue development in dnTNF and RID tg mice

(A) Representative Picrosirius red stain of IWAT from 8-week old C57B6 males on chow and after 9 day with HFD. (B) Representative Trichrome stain and collagen levels in IWAT of HFD-fed male RID tg and wildtype mice. (C) Representative H&E stain of liver sections from 11 weeks HFD-fed male dnTNF tg and littermate control. (D) Liver fat quantified by CT and liver weight in 11 weeks HFD-fed male RID tg and wildtype controls. (E) Representative H&E stain of IWAT and GWAT sections and endomucin immune-stain of IWAT (bottom panels) and (with quantification shown in (F)) from 10-day old male RID tg

and wildtype pups. (G) Body weight, IWAT weight and adipocyte sizes in 10-day old dnTNF tg and littermate controls. Error bars represent SEM, a p-value <0.05 according to student t-test was considered as significant and is indicated by */#; **: p<0.01; ***: p<0.001 (*significantly different from WT, # significantly different from untreated controls of same genotype).

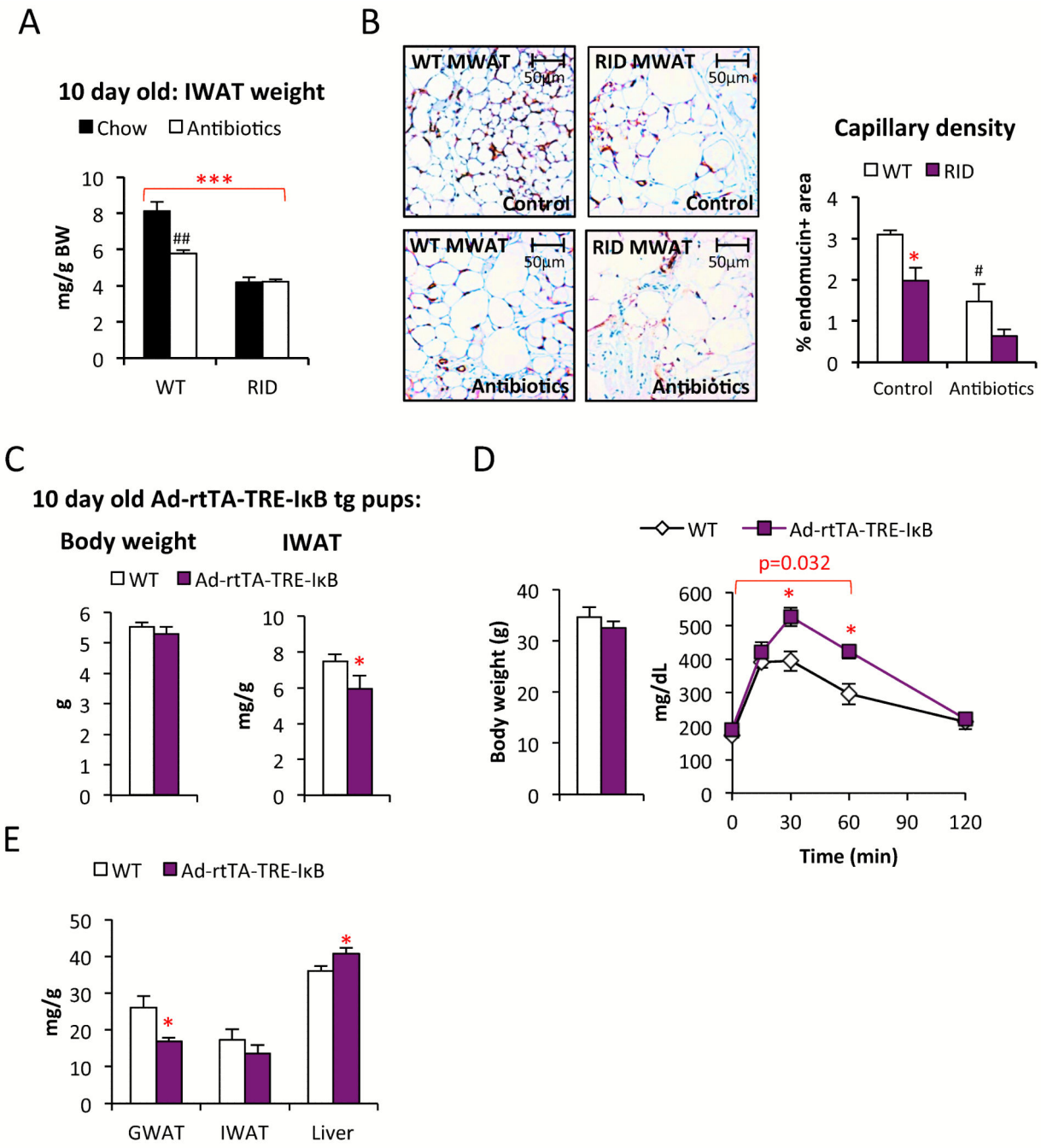

Figure 4. Ablation of gut microbiota affects capillary density and Ad-rtTA-TRE-IκB tg mice display reduced adipogenesis and glucose tolerance

(A) Effect of antibiotics-treatment on IWAT weight in 10-day old RID tg and wildtype pups. 1-way ANOVA analysis shows that both treatment ($F=5.3$, $p=0.026$) and genotype ($F=29.4$, $p<0.001$) contribute significantly to the IWAT weight. (B) Effect of antibiotics-treatment on capillary density in MWAT as judged by endomucin immune-stain in male RID tg and wildtype mice. 1-way ANOVA analysis shows that both treatment ($F=35.1$, $p=0.002$) and genotype ($F=14.8$, $p=0.012$) contribute significantly to capillary density in MWAT. (C) Body weight and IWAT weight in doxycycline-treated 10-day old Ad-rtTA-TRE-IκB tg and

littermate controls. (D) Body weight and glucose tolerance in 8-weeks HFD-fed male Ad-rtTA-TRE-IκB tg and littermate controls. (E) Dissected tissue weight in 8-weeks HFD-fed Ad-rtTA-TRE-IκB tg and littermate controls. Error bars represent SEM, a p-value <0.05 according to student t-test was considered as significant and is indicated by */#; **/##: p<0.01; ***: p<0.001 (*significantly different from WT, # significantly different from untreated controls of same genotype). P-value in red indicates difference between groups during the indicated time course according to repeated measurement ANOVA).

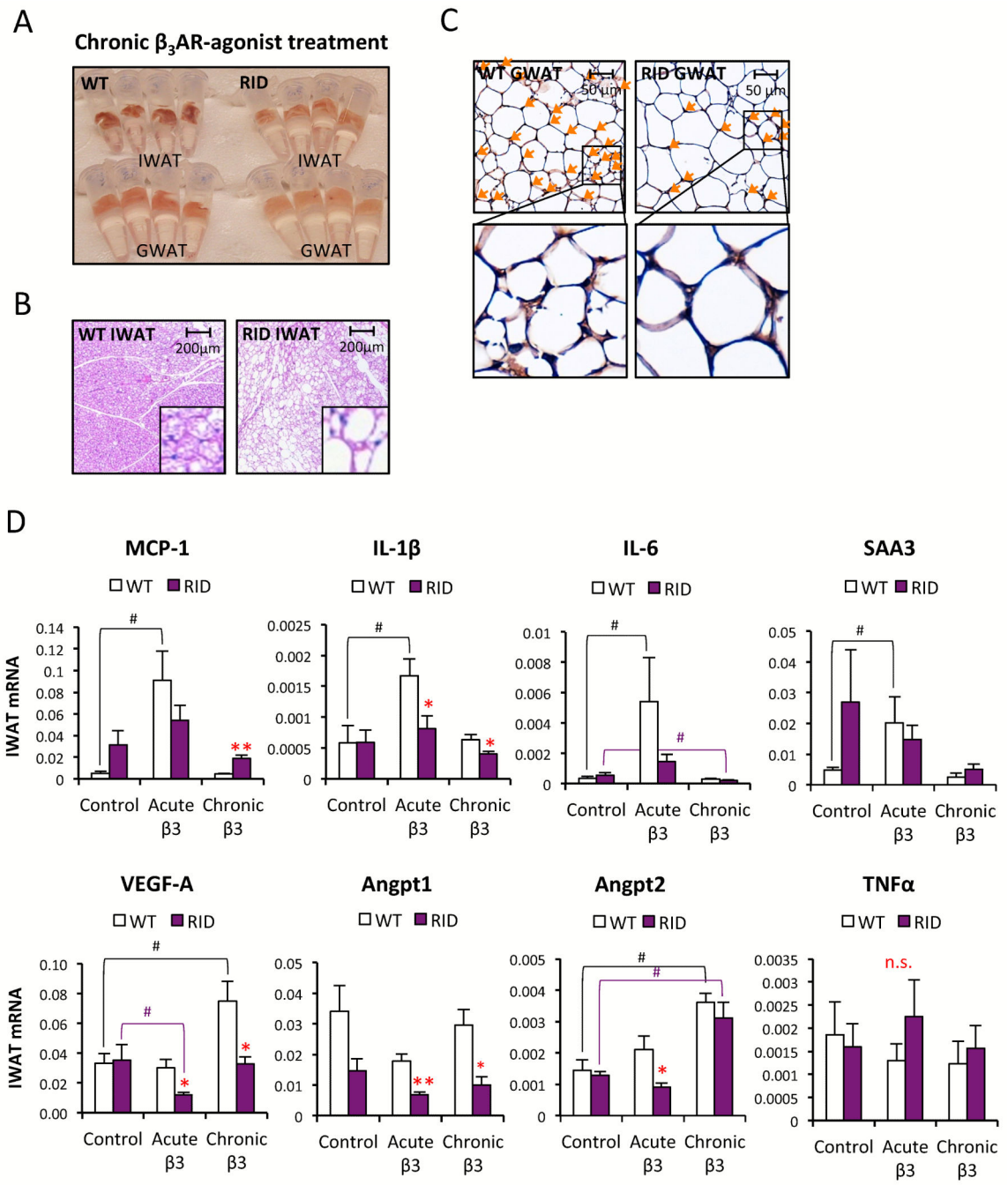

Figure 5. Reduced β_3AR-agonist-induced browning of white adipose tissue in RID tg mice

(A) Photo of IWAT and GWAT harvested from male RID tg and wildtype mice after chronic β_3AR-agonist treatment (10 days with daily i.p injection with 1mg/kg in PBS). (B) Representative H&E stain of IWAT from male RID tg and wildtype mice after chronic β_3AR-agonist treatment. (C) Representative BrdU immunostain of GWAT harvested after chronic β_3AR-agonist treatment (co-administered with 10 mg/kg BrdU) in male RID tg and wildtype mice. Orange arrows points towards BrdU positive nuclei (D) Gene expression analyses of IWAT 3 h (acute) after β_3AR-agonist injection and after chronic treatment

(IWAT harvested 24 h after last injection) in male RID tg and wildtype mice. Error bars represent SEM, a p-value <0.05 according to student t-test was considered as significant and is indicated by */#; **/##: p<0.01 (*significantly different from WT, # significantly different from untreated controls of same genotype). Additional 1-way ANOVA analyses have been performed for Figure 4D (Table S3)

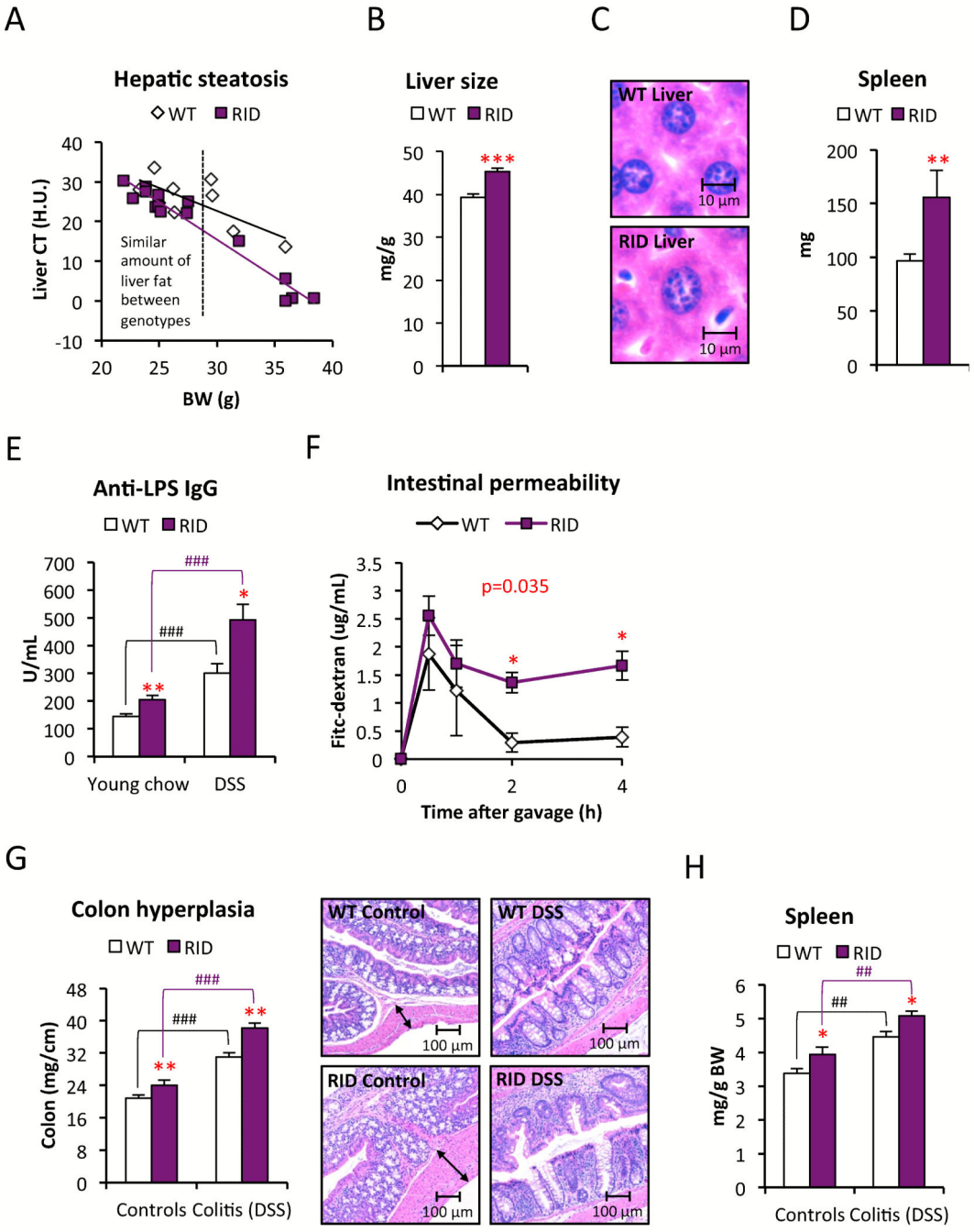

Figure 6. Leaky gut and colitis associated with signs of systemic inflammation in RID tg mice

(A) Liver fat quantified by CT in chow-fed male RID tg and wildtype mice. (B) Liver weight and (C) representative H&E stain of liver sections to show hepatocyte size in chow-fed male RID tg and wildtype mice with a body weight <30g. (D) Spleen size in chow-fed RIDs chow-fed male RID tg and wildtype mice. (E) Serum levels of anti-LPS IgG in young chow-fed vs. DSS-treated male RID tg and wildtype mice. 1-way ANOVA analysis shows that both treatment ($F=78.8$, $p<0.001$) and genotype ($F=26.4$, $p<0.001$) contribute significantly to anti-LPS IgG levels (F) Serum levels of FITC-dextran after an oral load in

young chow-fed female RID tg and wildtype mice. (G) Colon weight/length ratios, representative H&E images of colon and (H) spleen weight in untreated, and in response to DSS treatment, in male RID tg and wildtype mice. 1-way ANOVA analysis shows that both treatment ($F=153.6/47.3$, $p<0.001/<0.001$) and genotype ($F=27.4/13.9$, $p<0.001/0.05$) contribute significantly to both colon thickness and spleen size. Error bars represent SEM, a p-value <0.05 according to student t-test was considered as significant and is indicated by */#; **/##: $p<0.01$; ***/###: $p<0.001$ (*significantly different from WT, # significantly different from untreated controls of same genotype). P-value in red indicates differences between groups during time course according to repeated measurement ANOVA.

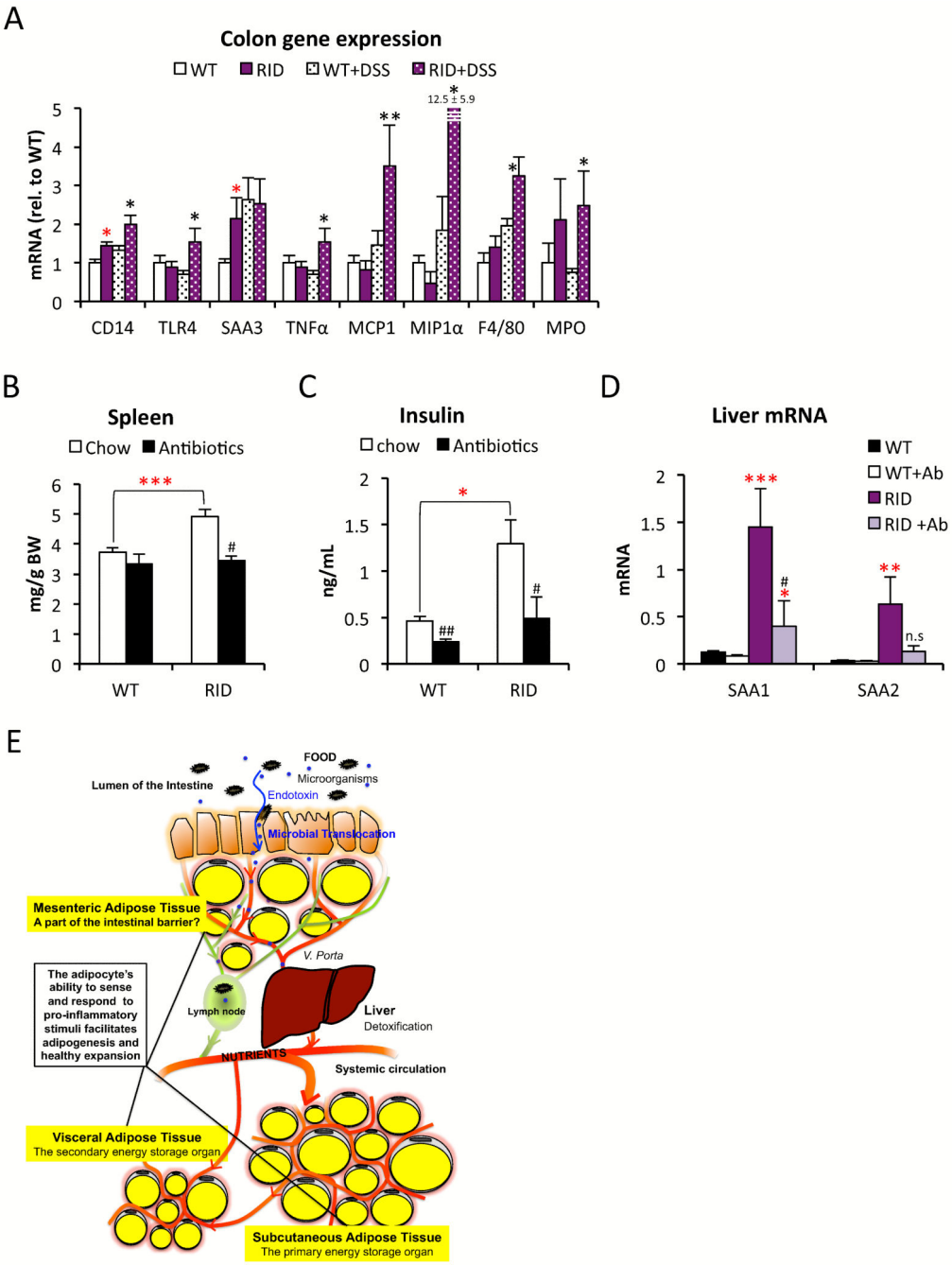

Figure 7. Antibiotics-treatment improves the RID tg mouse phenotype

A) Gene expression analysis of proximal colon in untreated, and in response to 3 DSS treatments, in male RID tg and wildtype mice. (B) Spleen, (C) fasting serum-insulin and (D) SAA1 and 2 mRNA levels in liver in control or antibiotic-treated male RID tg and wildtype mice. 1-way ANOVA analysis shows that both treatment (F=15.8/8.7/12.1/5.8, p=0.001/0.003/0.004/0.03) and genotype (F=19.3/17.1/23.6/31.8, p<0.001/0.001/<0.001/<0.001) contribute significantly to spleen size, insulin levels, liver SAA1 and liver SAA2 levels. (E) Summary and proposed model: Acute inflammation is essential for healthy

adipose tissue expansion and proper remodeling. Inability of adipose tissue to accurately sense and respond to inflammatory stimuli leads to reduced adipose tissue expansion and an increased risk for microbial translocation. Error bars represent SEM, a p-value <0.05 according to student t-test was considered as significant and is indicated by */#; **/##: p<0.01; ***: p<0.001 (*significantly different from WT, # significantly different from untreated controls of same genotype).